Atmospheric
Measurement
Techniques

Surface matters: limitations of CALIPSO V3 aerosol typing in coastal regions

T. Kanitz[1], A. Ansmann[1], A. Foth[2], P. Seifert[1], U. Wandinger[1], R. Engelmann[1], H. Baars[1], D. Althausen[1], C. Casiccia[3], and F. Zamorano[3]

[1]Leibniz Institute for Tropospheric Research, Permoserstr. 15, 04318 Leipzig, Germany
[2]Leipzig Institute for Meteorology, University of Leipzig, Stephanstr. 3, 04103 Leipzig, Germany
[3]Ozone and RUV Laboratory, Universidad de Magallanes, Punta Arenas 6210427, Chile

Correspondence to: T. Kanitz (kanitz@tropos.de)

Abstract. In the CALIPSO data analysis, surface type (land/ocean) is used to augment the aerosol characterization. However, this surface-dependent aerosol typing prohibits a correct classification of marine aerosol over land that is advected from ocean to land. This might result in a systematic overestimation of the particle extinction coefficient and of the aerosol optical thickness (AOT) of up to a factor of 3.5 over land in coastal areas. We present a long-term comparison of CALIPSO and ground-based lidar observations of the aerosol conditions in the coastal environment of southern South America (Punta Arenas, Chile, 53° S), performed in December 2009–April 2010. Punta Arenas is almost entirely influenced by marine particles throughout the year, indicated by a rather low AOT of 0.02–0.04. However, we found an unexpectedly high fraction of continental aerosol in the aerosol types inferred by means of CALIOP observations and, correspondingly, too high values of particle extinction. Similar features of the CALIOP data analysis are presented for four other coastal areas around the world. Since CALIOP data serve as important input for global climate models, the influence of this systematic error was estimated by means of simplified radiative-transfer calculations.

1 Introduction

The spaceborne Cloud-Aerosol LIdar with Orthogonal Polarization (CALIOP; Winker et al., 2009) has acquired a unique, global vertically resolved data set on aerosols and clouds within the framework of the Cloud-Aerosol Lidar Infrared Pathfinder Satellite Observation (CALIPSO) mission since 2006. Among the great successes of CALIPSO are, for example, the first global vertical distribution of atmospheric dust as presented by Liu et al. (2008) and a product for further height-resolved simulations of the aerosol radiative effect on the Earth's radiation budget (Huang et al., 2009).

Since the beginning, a great deal of effort has been invested in the validation of the CALIOP observations. The vertical aerosol distribution as derived with CALIOP agrees well with ground-based and airborne lidar observations (e.g., Mamouri et el., 2009; Pappalardo et al., 2010; Rogers et al., 2011). The aerosol optical thickness (AOT) of dust plumes as derived with CALIOP and in the framework of Aerosol Robotic Network (AERONET) has shown good agreement in the Mediterranean (Schuster et al., 2012). However, discrepancies in the extinction coefficient have been reported, especially for Saharan mineral dust (Wandinger et al., 2010; Tesche et al., 2013), caused by an underestimated extinction-to-backscatter ratio (S_P) for Saharan dust, which has to be assumed in the CALIPSO data algorithm to determine the particle extinction coefficient (Young and Vaughan, 2009; Young et al., 2013).

In the general data analysis of CALIOP, observed atmospheric layers are determined with a selective, iterated boundary location algorithm (Vaughan et al., 2009). The defined atmospheric layers are further categorized as cloud or aerosol layer (Liu et al., 2009). In the case of an aerosol layer a suitable S_P has to be found to determine the particle extinction coefficient. Therefore a subsequent algorithm is based on a yes/no decision tree with regard to the

aerosol-layer-integrated backscatter coefficient, the approximated particle linear depolarization ratio, and the altitude of the aerosol layer. In addition, the surface type information (e.g., snow and ice, desert, and water or land surface) below the footprint of CALIOP is used in the aerosol type identification. The possible aerosol types are clean marine (with $S_P = 20$ sr at 532 nm), clean continental ($S_P = 35$ sr), pure dust ($S_P = 40$ sr), polluted dust ($S_P = 55$ sr), polluted continental ($S_P = 70$ sr), and smoke ($S_P = 70$ sr) (details of the aerosol type identification in Fig. 2 of Omar et al., 2009; Lopes et al., 2013). These aerosol types and their S_P have been subject of numerous field campaigns (e.g., Burton et al., 2012; Groß et al., 2013).

The aerosol typing of CALIOP has been validated within various studies. For example, Burton et al. (2013) compared the aerosol typing of the backscatter lidar CALIOP with an airborne advanced high-spectral-resolution lidar. In coastal regions, the authors found a bias toward too low extinction values in the CALIPSO data over water, because the CALIPSO data algorithm determined clean marine aerosol although terrestrial aerosol was transported to the sea and increased the absorptivity of the marine boundary layer. Such findings were reported in the framework of ground-based investigations as well (Schuster et al., 2012; Bridhikitti et al., 2013; Omar et al., 2013) and synergistic satellite observations (Oomar and Holz, 2011).

Here, we report on another aspect of the CALIOP data analysis in coastal regions. Clean marine aerosol is only permitted over water surfaces (Omar et al., 2009). Hence, when CALIPSO crosses a coastal line (from sea to land), the S_P value immediately changes from 20 to 70 sr in the worst case, a jump from clean marine to smoke or polluted continental aerosol in the typing scheme. Correspondingly, abrupt changes in the particle extinction coefficients by a factor of up to 3.5 can occur, as will be shown below. Thus, an overestimation of the particle extinction coefficients over land within the zone that is affected from advection from ocean to land (≈ 100 km onshore; Miller et al., 2003) must be taken into account when studying aerosol conditions in coastal areas. This applies to the extinction coefficient in the CALIOP level 2 data and vice versa to CALIOP level 3 products. Consequently, it could explain the positive bias between CALIOP level 3 AOT data and sun-photometer-derived AOT at coastal sites, which was shown in Winker et al. (2013).

In the present study, ground-based lidar observations of Polly^{XT} (Althausen et al., 2009) conducted during a four-month campaign at Punta Arenas and data sets of CALIOP lidar and AERONET photometer observations were used to establish an aerosol climatology for the region around Punta Arenas, the most southern tail of southern South America. These measurements offered an excellent opportunity to validate CALIOP aerosol observations in the complex orography of the highly structured coastal environment with fast changes between water and land surfaces in the very south of southern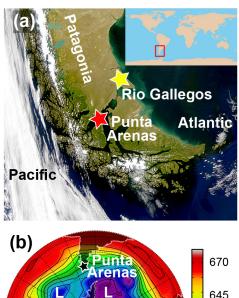 South America. In the same latitudinal belt the first Aerosol Characterization Experiment was performed to determine aerosol background conditions for later investigation (Bates et al., 1998). Continental aerosol sources are limited to a minimum, and simple, almost pure marine conditions with rather low AOT values can be assumed around Punta Arenas so that any bias in the CALIPSO data analysis sensitively shows up and can be identified.

An introduction to the campaign at Punta Arenas is given at the beginning of Sect. 2. Afterwards, the instruments are briefly explained. In Sect. 3.1, we discuss a case study of collocated measurements with Polly^{XT} and CALIOP in the area of Punta Arenas. Clear evidence of a misclassified aerosol layer within the CALIOP aerosol typing due to changes in the underlying surface type is presented. A larger set of observations from CALIOP is contrasted with combined Polly^{XT} and AERONET sun photometer measurements in Sect. 3.2 to evaluate the influence of the underlying surface on the aerosol climatology from CALIOP for the area of Punta Arenas. We complement our findings with further examples of other CALIOP measurements in coastal environments including observations at Hawaii (Pacific), Tasmania (Pacific), Ireland (Atlantic), and Cuba (Atlantic, Sect. 3.3). In Sect. 3.4 simplified radiative-transfer calculations were performed for clean marine and polluted conditions in the planetary boundary layer. Finally, a summary of the findings is given in Sect. 4.

2 Experiment

2.1 Field site

The mobile facility OCEANET-Atmosphere of the Leibniz Institute for Tropospheric Research (TROPOS) performs aerosol and cloud observation with a Raman/polarization lidar on a regular basis during the meridional transatlantic cruises of the research vessel *Polarstern* between northern and southern midlatitudes (Kanitz et al., 2013). While *Polarstern* moved on to Antarctica during the southern hemispheric summer of 2009/2010, the time period between the tracks (26 November 2009–17 April 2010) was used to perform aerosol observations with lidar at Punta Arenas, Chile ($53°$ S, $71°$ W). In the framework of the ALPACA (Aerosol Lidar measurements at Punta Arenas in a Chilean germAn cooperation) campaign from 4 December 2009 to 4 April 2010, the TROPOS lidar Polly^{XT} was deployed at the Universidad de Magallanes. Punta Arenas is located at the Strait of Magellan (Fig. 1a). In the west direction rugged spurs of the Andes and in the east direction grassy fields dominate the orography. Constant westerly to northwesterly air flows prevail throughout the year with a mean surface speed of $4.6\,\mathrm{m\,s^{-1}}$, which is caused by the Antarctic low-pressure belt (Schneider et al., 2003). Figure 1b shows a map of the Southern Hemisphere. Geopotential height at 500 hPa is denoted by the color code for 1 January 2010
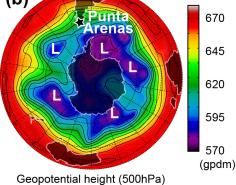
Figure 1. (a) Map of the southern part of South America. **(b)** Map of the Southern Hemisphere. Geopotential height at 500 hPa is shown by the color code for 1 January 2010. L denotes low-pressure system. Punta Arenas is indicated by a red star in **(a)** and a black star in **(b)**, and Rio Gallegos by a yellow star in **(a)**.

in Fig. 1b. Dark colors indicate the low-pressure systems around the Antarctic. Air masses are advected along the isohypses (black contour lines in Fig. 1b). As it is clearly shown in Fig. 1b, the air masses that are advected to Punta Arenas pass over no other continental areas and are usually of pure marine origin.

Close to Punta Arenas, AERONET observations have been performed 200 km northeast in Rio Gallegos, Argentina, at the Atlantic coast, further downwind from Punta Arenas, since November 2005 (Fig. 1a). The meteorological conditions are similar at Rio Gallegos and at Punta Arenas.

2.2 Polly^{XT}

Polly^{XT} measures backscattered light at wavelengths of 355, 532, and 1064 nm and inelastically Raman-scattered light at 387 and 607 nm in order to determine profiles of the particle backscatter coefficient at three wavelengths and the extinction coefficient at 355 and 532 nm. A polarization-sensitive channel detects light at 355 nm and allows for the determination of the particle linear depolarization ratio (Freudenthaler

et al., 2009). Polly^{XT} data are acquired at a vertical and temporal resolution of 30 m and 30 s, respectively. The system was operated 24/7 and controlled remotely by TROPOS via internet access during the whole campaign.

In the analysis of the observations, we had to deal with two limitations of the instrument. In the near range (< 400 m), the signal of the bistatic system is affected by an incomplete overlap of the laser beam with the receiver field of view. As a consequence, values of the particle backscatter coefficient were set constant below 400 m height based on the planetary boundary layer height. In doing so, we assume well-mixed conditions in the lower part of the planetary boundary layer, which was found to be sufficient under marine conditions (Kanitz et al., 2013).

In addition, the UV channels did not work properly during ALPACA. The backscatter coefficient at 532 nm was determined from the ratio of the inelastic and elastic backscatter signal (Ansmann and Müller, 2005). But because of the rather low aerosol content, the inelastic signals could not be used for direct extinction-coefficient profiling. The particle extinction coefficient had to be estimated from the 532 nm backscatter coefficient by means of appropriate S_P values in combination with AERONET sun photometer observations of the total atmospheric AOT. Accounting for the spatial separation of the two measurement sites, HYSPLIT trajectory analyses (Draxler and Rolph, 2003) and an aerosol transport model (namely the Navy Aerosol Analysis and Prediction System, NAAPS) were incorporated to align lidar and sun photometer observations. A simplified statistical approach will be discussed in Sect. 3.2.

2.3 AERONET sun photometer

An AERONET (Holben et al., 1998) station is located at Rio Gallegos, Argentina (CEILAP-RG). The AERONET sun photometer measures AOT (column-integrated extinction coefficient) from 340 to 1020 nm at 7 channels. In our analysis we used the level 2.0 data. The uncertainty in the AOT values is 0.01–0.02 (Holben et al., 2001).

2.4 CALIOP

CALIOP is an elastic-backscatter lidar that orbits the Earth at a height of 705 km with a velocity of 7000 m s^{-1}. Based on the laser footprint the lidar covers 0.2 % of the Earth's surface during one repeat cycle (Kahn et al., 2008). It passes over the same location every 16th day. CALIOP measures backscattering at 532 and 1064 nm and depolarization at 532 nm. The system and data analysis is explained by Winker et al. (2009). Within the present study, we focus on the level 2, version 3 data obtained for the wavelength of 532 nm. The level 2 data provide profiles of the particle backscatter and extinction coefficient, as well as information about the determined feature type (e.g., clouds or aerosols) and aerosol subtype (e.g., dust,

smoke). Furthermore, quality flags are provided for each data point.

We used the cloud–aerosol discrimination (CAD) score (Liu et al., 2009), the feature classification flags (Omar et al., 2009), and the extinction flag (Young and Vaughan, 2009) for the data quality assurance. We set conservative thresholds of CAD score ≤ -90 (observed layer is likely to contain aerosols with very high probability; optically thin marine boundary layer clouds are avoided), feature subtyping flag $= 1$ (confident aerosol subtyping), and extinction flag $= 0$ (no changes in S_P within the hybrid extinction retrieval algorithm are allowed). The obtained surface type is given by the International Geosphere-Biosphere Programme (IGBP, 1990) map and the position information of CALIOP itself.

2.5 Library for radiative transfer (libRadtran)

Radiative-transfer calculations were performed with the UVSPEC program (Kylling, 1992) of the libRadtran library version 1.6 beta (Mayer and Kylling, 2005). Broadband solar downward and upward irradiances were calculated from 245 to 4500 nm wavelength to estimate the direct solar aerosol radiative effect (SARE) at the surface and the top of the atmosphere (TOA). The libRadtran library includes the spectral integration by the correlated-k approximation (Kato et al., 1999) and the discrete ordinate solver DISORT version 2.0 (Stamnes et al., 1988). DISORT was applied with 16 streams. Solar zenith angles were determined as a function of latitudinal belt (10° steps from 50° N to 50° S), season (15th of January, April, July, and October), and in steps of 15 min per day (Blanco-Muriel et al., 2001). Aerosol-free and cloud-free atmospheric conditions were described with US standard atmosphere (Anderson et al., 1986) as implemented in libRadtran for trace gases, pressure, temperature, and relative humidity. Aerosol single-scattering albedo and asymmetry parameter were taken from Dubovik et al. (2002).

3 Results

We begin with a case study of a homogeneous aerosol layer observed with Polly[XT] and CALIOP in the area of Punta Arenas. The patterns found in the CALIOP aerosol subtype mask will show evidence of a surface-dependent aerosol characterization within the CALIOP data algorithm. Afterwards, the general aerosol conditions in the area of Punta Arenas will be analyzed based on the ground-based Polly[XT] observations and AERONET long-term monitoring. The results will be contrasted with the CALIPSO long-term measurements to examine the impact of the surface-related effect on the CALIPSO-derived aerosol statistics. We will finish the analysis with further CALIOP observations in rather different coastal environments to corroborate our case study analyses at Punta Arenas. A simplified study on the influence of
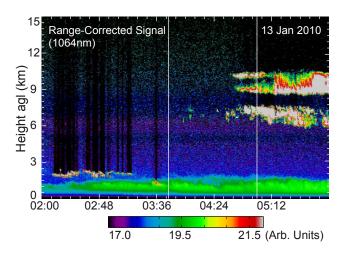

Figure 2. Height–time display of the range-corrected 1064 nm signal measured with Polly[XT] at Punta Arenas on 13 January 2010, 02:00–06:00 UTC (night). White lines indicate the time period from 03:45 to 05:00 UTC as chosen for the comparison with the CALIOP measurement (see Fig. 3b).

aerosol mistyping on radiative-transfer calculations will be presented at the end.

3.1 A case study of artificial patterns in a homogeneous aerosol layer

Figure 2 shows the observation of Polly[XT] for the period from 02:00 to 06:00 UTC on 13 January 2010. Patterns of clouds at 2, 7, and 10 km height as well as an aerosol layer reaching to 1.5 km height can be seen. Within this measurement period CALIPSO passed over Punta Arenas at a distance of about 150 km, indicated by a thin red line and a red star in Fig. 3a. In addition, grey areas show water surfaces and bright areas land surfaces as determined within IGBP. In the surrounding of Punta Arenas, grey areas indicate the rugged coastline and the large water surfaces of the Strait of Magellan (see also Fig. 1a). The vertical distribution and structure of the cloud and aerosol layers in the selected data subset of CALIOP (thick red line in Fig. 3a) is in excellent agreement with the patterns of the Polly[XT] observation (cf. Figs. 2 and 3b).

Figure 3c presents the feature type mask of the data subset for the period indicated by the box with white borders in Fig. 3b (from 54 to 52° S). Green coloring and dark blue coloring in Fig. 3c indicate the surface elevation and aerosol-free atmosphere, respectively. Data points for which no aerosol and cloud information could be retrieved due to strong attenuation of the laser beam are colored black. Data points of uncertain feature type are colored red. In the beginning of the measurement period aerosol (orange) was identified up to 1.5 km below clouds (light blue) and even within the clouds. The subtype mask in Fig. 3d shows abrupt changes between mainly polluted continental aerosol (with
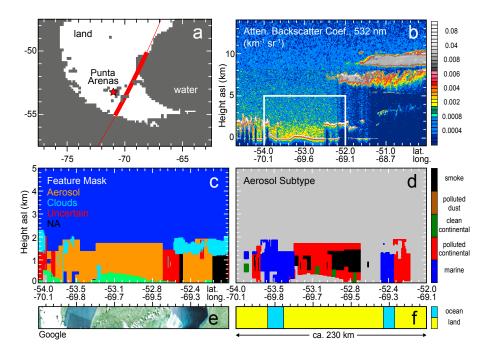
Figure 3. (a) Map of the southernmost part of South America. The thin red line shows the CALIOP night overflight on 13 January 2010. The red star indicates Punta Arenas. The thick red-line segment indicates the selected time period of CALIOP in best agreement to the Polly^{XT} observation. **(b)** Height–time display of the lidar attenuated backscatter at 532 nm of the CALIOP observation at 04:47 UTC on 13 January 2010 (for the thick red-line period in **a**). **(c)** Height–time display of the vertical feature mask and **(d)** the aerosol subtype mask of the highlighted data subset in **(b)**. Surface type information from the **(e)** Google Earth map and **(f)** the International Geosphere-Biosphere Programme (IGBP, 1990).

smoke embedded) and marine aerosol from left to right, indicated by the change between red and blue. We added the surface type information in terms of a Google Earth map (Fig. 3e) and from the IGBP map (Fig. 3f). In Fig. 3f, yellow sections indicate land surfaces and light-blue sections indicate water surfaces. The change in the determined aerosol type from polluted continental aerosol to marine aerosol is associated with the change in the surface type from land to ocean, and in consideration of the spatial averaging in the CALIOP data. The switch from red/black to blue columns can be observed two times in the course of the measurement on 13 January 2010 (Fig. 3d), although the height–time display of the CALIOP-derived attenuated backscatter (Fig. 3b) indicates a homogeneous boundary-aerosol layer, similar to the higher temporal and vertically resolved measurement of Polly^{XT} (Fig. 2).

Particle backscatter coefficients from CALIOP level 2 data for cloud-free signals were selected for the scene shown in Fig. 3d to avoid an effect from cloud contamination in the data (Yang et al., 2012; Varnai et al., 2013). Figure 4a presents profiles of the particle backscatter coefficient at 532 nm determined with Polly^{XT} (green line, 30 m vertical resolution with 330 m vertical smoothing) and CALIOP (black line, 60 m vertical resolution). The black curve differs only slightly from the green curve in magnitude. Figure 4b shows the mean profiles of the particle backscatter
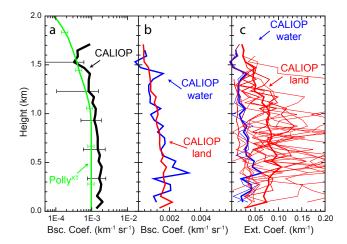

Figure 4. (a) Mean vertical profiles of the particle backscatter coefficient at 532 nm as determined with Polly^{XT} (green) from 03:45 to 05:00 UTC and CALIOP at around 04:47 UTC on 13 January 2010. The CALIOP backscatter profiles are based on cloud-free signal profiles (black). **(b)** Averaged cloud-free profiles of the particle backscatter coefficient at 532 nm over land (red) and over water surface (blue) determined from CALIOP measurements. **(c)** Averaged cloud-free profiles of the extinction coefficient at 532 nm (thick lines) and individual profiles (thin lines).
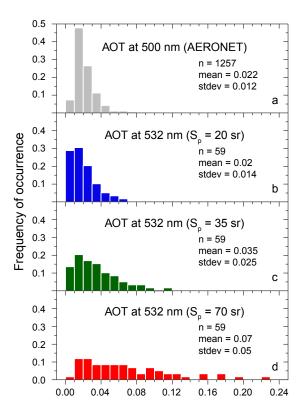
Figure 5. Frequency of occurrence of AOT from **(a)** AERONET sun photometer measurements at Rio Gallegos (level 2.0, 1257 cases), and **(b–d)** from Polly[XT] measurements at Punta Arenas (59 cases) for S_P of 20, 35, and 70 sr, representing clean marine, clean continental, and smoke or polluted aerosol conditions, respectively, from 4 December 2009 to 4 April 2010.

Figure 6. International Geosphere–Biosphere Programme (IGBP, 1990) surface type map of southern South America and selected CALIOP cross sections within 200 km of Punta Arenas.

coefficient as derived with CALIOP measurements over water (blue) and over land (red) without clouds. The profiles indicate similar backscatter conditions over land and water. In contrast to the two particle backscatter profiles, the respective mean extinction coefficients deviate strongly. Over the water surface the aerosol layer is identified as marine aerosol and the backscatter coefficients are multiplied by S_P of 20 sr. However, over land the aerosol layer was interpreted partly as polluted continental aerosol, partly as smoke, and sometimes as clean continental aerosol. Thus, the extinction coefficients are computed from the backscatter coefficients by using $S_P = 35$ sr (clean continental) and mostly $S_P = 70$ sr (polluted continental and smoke). As a result, the extinction coefficients determined in a more or less homogeneous aerosol layer over land are about 3.5 times higher than over water surface (Fig. 4c).

3.2 A possible overestimation of strong absorbing continental aerosol at Punta Arenas

The surface-type dependence of the aerosol typing within the CALIOP data algorithm may affect general long-term aerosol studies with CALIOP at coastal regions. In the
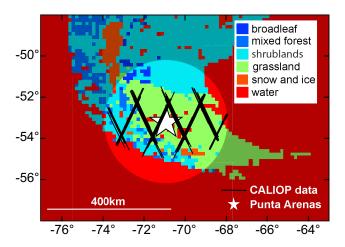
framework of ALPACA the ground-based lidar observations of Polly[XT] at Punta Arenas and the AERONET sun photometer observations at Rio Gallegos were used to determine the AOT frequency distribution for the period from 4 December 2009 to 4 April 2010 during cloud-free conditions.

Within this approach, the lidar profiles of the particle backscatter coefficient were vertically integrated and multiplied with S_P of 20, 35, and 70 sr, representing marine, clean continental, and polluted continental aerosol, respectively. Figure 5a shows the AOT frequency distribution as derived with sun photometer at Rio Gallegos. In > 95 % of all cases, the AOT is < 0.05. Assuming almost similar aerosol conditions at Punta Arenas and Rio Gallegos, the lidar-derived AOT distribution determined with a S_P of 20 sr shows the best agreement with the AERONET-derived AOT distribution. The assumption of the presence of polluted continental aerosol or smoke, so that S_P of 70 sr is appropriate, leads to an unrealistic AOT statistics for this rather clean environment (Fig. 5d). The very low annual AOT of ≈ 0.02 (2009, 2010) from AERONET observations indicates clean marine conditions as well (Smirnov et al., 2009; Wilson and Forgan, 2002).

In the next step, CALIOP level 2, version 3 data were analyzed for the ALPACA campaign. For CALIPSO overflights within a distance of 200 km to Punta Arenas (Anderson et al., 2003) HYSPLIT trajectory analyses enabled us to select the part of the CALIPSO track that relates best to the 24/7 measurements of Polly[XT] at Punta Arenas (Tesche et al., 2013). A cross section was defined to consist of 40–50 profiles in order to account for frequently occurring clouds (Kanitz et al., 2011) that totally attenuate the laser beam of the spaceborne lidar and prohibit aerosol investigations below. After quality screening, a very small number of cases (28) remained. Thus, under consideration of almost constant meteorological conditions throughout the year, the time period was extended
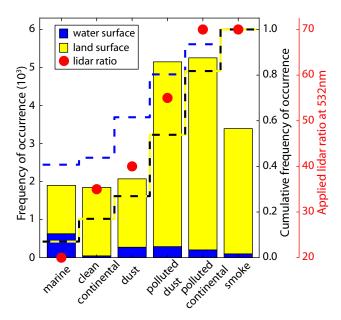
Figure 7. Frequency of occurrence of aerosol types as determined with CALIOP from 1 May 2009 to 31 April 2010 within a distance of 200 km around Punta Arenas. Blue coloring denotes cases over water surface, and yellow colors indicate cases over land surface. The cumulative frequency is given by dashed blue (water) and yellow–black lines (land). Red dots show the aerosol-type-related S_P.

to 1 May 2009–31 April 2010 in the analysis to achieve a reasonable number of CALIPSO data subsets. Finally, in 16 out of all 142 cases (11 %) the trajectory analysis eliminated the data from further consideration, because the interceptions were more than 200 km away from Punta Arenas or no data were available. The selected cross sections are shown in Fig. 6. Ninety-one cases (64 %) remained after quality-assurance tests as described above. Figure 7 presents the frequency of occurrence of aerosol types as determined with CALIOP. Polluted continental aerosol and polluted dust were most often determined with CALIOP in the area of Punta Arenas. Taking Fig. 6 into consideration, a high fraction of profiles was acquired over land surface and only a minor fraction over water surface, in particular the Strait of Magellan. Stacked bars in Fig. 7 show the number of observations over water surface (blue) and land surface (yellow) for each aerosol type. Cumulative frequency curves (dashed lines) indicate the fraction of the observed aerosol types over water (blue–white) and land surface (yellow–black). Over water surface, marine aerosol was found in about 41 % of all cases, while over land surface it was determined in only 7 % of all cases and within the distance of the horizontal averaging in the CALIOP data algorithm off the water surface. Over water and land, 38 and 73 %, respectively, of aerosols were identified as either smoke, polluted dust, or polluted continental aerosol ($S_P \geq 65$ sr). These findings show a clear contradiction between the CALIOP retrieval over land and the

ground-based observations as presented in Fig. 5. The analysis was repeated for cases north ($< 53°$ S) and south of Punta Arenas to consider the influence of the Patagonian Desert (Fig. 1). In 52 and 33 % of all cases, marine aerosol was found over water surface in the north and south of Punta Arenas. Over land surface the CALIOP retrieval identified marine aerosol in only 5 and 9 % of all cases. In contrast, absorbing aerosol (S_P of 55–70 sr) was found in 37 % (74 %) and 40 % (72 %) of all cases over water (land) in the north and south. If the entire analysis is restricted to boundary-layer aerosol (height < 1 km), marine aerosol is determined in 48 % of all cases over water surface and in 11 % of all cases over land surfaces. However, strong absorbing aerosol was found more often over land surface (71 %) than over water surface (38 %). The statistical analysis shows a high contribution of continental aerosols to the general aerosol content in the surrounding of Punta Arenas, although from the intensive and permanent ocean-to-land advection a reasonable contribution of clean marine would be expected aerosol in this area. According to the measurements of CALIOP, clean continental aerosol, which is closest to the marine aerosol in terms of the lidar ratio (35 and 20 sr), is of minor impact in the surrounding of Punta Arenas. The ground track of CALIPSO crosses mainly grasslands, shrublands, and forests (see Fig. 6). Considering these three surface types, the decision tree in Omar et al. (2009) indicates that clean continental aerosol is determined if the aerosol-layer-integrated backscatter coefficient is smaller than 0.0005. If this is not the case, polluted continental aerosol or smoke are determined.

3.3 CALIOP aerosol typing at other coastal regions

Further examples of CALIOP measurements in coastal regions and under aerosol background conditions are presented in Fig. 8. The abscissa in Fig. 8a–h show the coordinates of the CALIPSO flight track in terms of latitude (upper row, south < 0) and longitude (lower row, west < 0). On 24 December 2009 (nighttime) CALIPSO passed over Mauna Loa, Hawaii (Fig. 8a). According to the CALIOP level 2 data, marine aerosol was observed around Mauna Loa, indicated by blue color in Fig. 8e. As soon as CALIOP measured over land, the boundary-layer aerosol was classified as smoke and polluted continental aerosol. As explained before, the change in the aerosol type is associated with the use of a significantly increased S_P value. Figure 8i shows the averaged profiles of the 532 nm backscatter and extinction coefficients by dashed and solid lines, respectively, for the aerosol conditions in Fig. 8e. Blue and red lines indicate profiles acquired over water and land surface, respectively. The error bars are the root-mean-squared error provided in the CALIOP level 2 data for each profile. Although the backscatter coefficients show almost equal values from 1 to 2 km height, the extinction coefficients show a difference of a factor of 3–4. The same pattern can be seen in terms of an overflight of CALIPSO
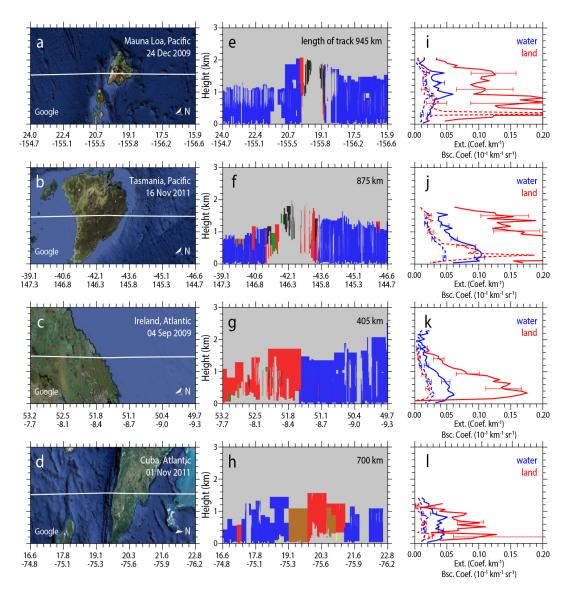
Figure 8. (a–d) Surface type information from Google Earth map of different coastal areas. Flight tracks of selected CALIPSO overflights are indicated by the white lines. Axis numbers show the coordinates of the flight track (upper row: latitude, lower row: longitude). **(e–h)** Height–time display of the aerosol subtype mask as determined with CALIPSO during overflight of the location to the left. The length of the selected cross section is given at the right top. **(i–l)** Corresponding mean profiles of 532 nm backscatter (dashed) and extinction coefficient (solid) separately for water (blue) and land surface (red).

over Tasmania on 16 November 2011 (nighttime; Fig. 8b, f, and j). Two other measurement examples were taken from the CALIPSO data set in the area of the Atlantic Ocean. On 4 September 2009 (nighttime, Fig. 8k) and 1 November 2011 (daytime, Fig. 8l) CALIOP-retrieved profiles of the 532 nm backscatter coefficient over water and land surface are in good agreement and indicate homogeneous aerosol layers along the selected overflights of CALIPSO over Ireland and Cuba. Nevertheless, strong differences between the respective extinction values (over water versus over land) occurred due to the subtyping used in the CALIOP data analysis.

3.4 Radiative effect of marine and polluted aerosol

A simple assessment study was performed to estimate the solar aerosol radiative effect (SARE) of the planetary boundary layer for pure marine and polluted aerosol conditions. The difference in SARE (pure marine vs. polluted) indicates the magnitude of the bias in the aerosol radiative effect caused by the surface effect in the CALIOP data analysis at coastal sites. For both scenarios the boundary layer top was set to 0.8 km height, and well-mixed conditions (constant aerosol extinction profile) were assumed in the boundary layer. The AOT was set to 0.05 in the scenario
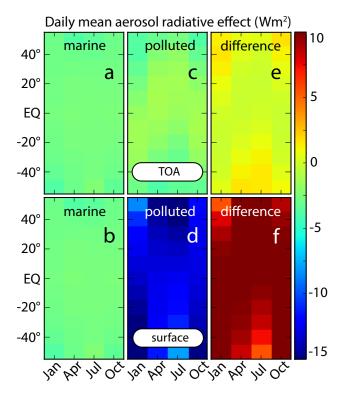
Figure 9. Direct solar aerosol radiative effect at the top of the atmosphere (TOA, top panel) and surface (bottom panel) for marine and polluted boundary-layer aerosol (left and center). Right: difference in the direct solar radiative effect of both aerosol scenarios.

Table 1. Input parameter for simplified radiative-transfer calculations. Mean aerosol optical thickness (AOT) for marine conditions is taken from Smirnov et al. (2009), single-scattering albedo (SSA) and asymmetry parameter (g) are taken from Dubovik et al. (2002).

Input for radiative-transfer calculations		
Scenario 1	AOT	0.05
(marine)	Ångström	0.4
	SSA (440/670/870/1020)	0.98/0.97/0.97/0.97
	g (440/670/870/1020)	0.75/0.71/0.69/0.68
Scenario 2	AOT	0.175
(polluted)	Ångström	0.8
	SSA (440/670/870/1020)	0.91/0.89/0.86/0.84
	g (440/670/870/1020)	0.74/0.67/0.64/0.63

Table 2. Results of radiative-transfer calculations for different surface albedos. Pure marine and polluted aerosol conditions were simulated at 0° latitude and longitude in spring (on 15 April). The settings for both scenarios are given in Table 1. TOA and SARE denote the top of the atmosphere and the 24 h averaged solar aerosol radiative effect.

	Scenario	Aerosol	SARE ($W\,m^{-2}$) for albedos		
			0.05	0.20	0.40
Surface	1	marine	−3.5	−2.5	−1.4
	2	polluted	−16.1	−12.7	−8.7
TOA	1	marine	−2.5	−1.4	−0.2
	2	polluted	−6.0	−1.3	4.8

of marine conditions on the basis of global sun photometer observations (Smirnov et al., 2009). In accordance with the CALIOP data algorithm, the AOT was defined 3.5 times higher, 0.175, in the scenario for polluted conditions. The information on single-scattering albedo and asymmetry parameters was taken from AERONET for marine aerosol and polluted continental aerosol, respectively, specifically the measurement results from Lanai and the Maldives (cf. Table 1 in Dubovik et al., 2002). Table 1 gives an overview for both scenarios. The surface albedo was set to 0.2 to represent surface conditions between deserts (0.2–0.45) and different vegetation (0.05–0.25).

Figure 9 (top and bottom panel) shows the SARE, determined using libRadtran of the boundary layer at the TOA and the surface for different latitudes and seasons, represented by the 15th of January, April, July, and October. At the TOA the SARE in both scenarios is almost similar and ranges from -1 to $-4\,W\,m^{-2}$ with season and latitude (Fig. 9 a and c). The difference in the SARE at the TOA (i.e., the impact of the different aerosol conditions on the SARE) is less than $2\,W\,m^{-2}$, as indicated in Fig. 9e. Consequently, the higher AOT and absorption (lower single-scattering albedo) in the scenario for polluted aerosol conditions in the boundary layer do not significantly alter the planetary albedo for incident radiation in comparison to pure marine conditions. In contrast,

the SARE at the surface shows large deviations for the simulations of both scenarios (Fig. 9b and d). In the scenario for polluted aerosol conditions, the higher AOT and the efficient absorption of incident radiation increases the SARE from a maximum of $-4\,W\,m^{-2}$ (marine conditions) to a maximum of $-17\,W\,m^{-2}$ (polluted conditions). The difference in the SARE ranges from 5 to $13\,W\,m^{-2}$ (Fig. 9f).

Additional simulations were performed for surface albedos of 0.05, 0.2, and 0.4 at 0° latitude and longitude on 15 April. Table 2 indicates the sensitivity of the surface albedo on the SARE at TOA. The difference of SARE at TOA for lower and higher surface albedos than 0.2 increases to $5\,W\,m^{-2}$ for a surface albedo of 0.4 (Table 2). In the case of a surface albedo of 0.4, the SARE changes from a cooling effect (negative SARE) of $-0.2\,W\,m^{-2}$ under marine conditions to a warming effect (positive SARE) of $4.8\,W\,m^{-2}$ for a boundary layer with polluted aerosol. At the surface, SARE decreases with increasing surface albedo for both aerosol conditions. The difference between the SAREs decreases from $-12.6\,W\,m^{-2}$ to $-7.3\,W\,m^{-2}$ for surface albedos from 0.05 to 0.4, respectively.

Table 3. Results of radiative-transfer calculations for different aerosol optical thickness (AOT). Pure marine and polluted aerosol conditions were simulated for a surface albedo of 0.2 at 0° latitude and longitude in spring (on 15 April). The settings for both scenarios are given in Table 1. TOA and SARE denote the top of the atmosphere and the 24 h averaged solar aerosol radiative effect.

	Scenario	Aerosol	AOT	SARE (W m^{-2})
Surface	1	marine	0.020	−1.0
	2	polluted	0.070	−5.5
	1	marine	0.050	−2.5
	2	polluted	0.175	−12.7
TOA	1	marine	0.020	−0.6
	2	polluted	0.070	−0.6
	1	marine	0.050	−1.4
	2	polluted	0.175	−1.3

The obtained simulation results shown in Fig. 9 represent worst-case scenarios based on the AOT of 0.05 for marine conditions (Smirnov et al., 2009). In the area of Punta Arenas, the mean AOT is below 0.05. Radiative-transfer calculations were repeated for both scenarios based on an AOT value of 0.02 for marine conditions at 0° latitude and longitude in spring, on 15 April, respectively. The AOT was set to 0.07 for polluted aerosol conditions. Table 3 presents the SARE for different aerosol conditions and AOTs. In agreement to Fig. 9 the SARE at TOA is almost similar for both scenarios and AOT values as found in the area of Punta Arenas if the simulations are performed for a surface albedo of 0.2 (cf. Table 2). At the surface SARE decreases with the decreased AOT (0.05–0.02) from −2.5 to −1.0 W m^{-2} for marine conditions and from −12.7 to −5.5 W m^{-2} for a boundary layer with polluted aerosol and AOTs of 0.175 to 0.07. Finally, the difference between both scenarios is 4.5 W m^{-2} for the approach with lower AOTs. In summary, a bias in studies of surface SARE cannot be excluded when aerosol conditions are based on CALIOP extinction profiles at coastal sites, as a consequence of the surface effect in the CALIOP data analysis.

4 Conclusions

By analyzing coincident measurements of the CALIOP lidar, AERONET sun photometer, and Polly[XT] lidar at the rugged coastline of southern South America, clean atmospheric background conditions (AOT of ≈ 0.02) were investigated which are representative of the latitudinal belt from 50 to 60° S. In this area, the Antarctic low-pressure belt advects constantly air masses from the southern oceans, and continental aerosol sources are almost absent. Consequently, AERONET and Polly[XT] observations revealed clean marine aerosol conditions mixed with local clean continental aerosol in southern South America. However, the automated

CALIOP data analysis classified the detected aerosol as polluted dust, polluted continental aerosol, or smoke in about 70 % of all cases. Within this case study, this discrepancy was found to be the result of the surface-dependent CALIOP data analysis, including the prohibition of marine aerosol over land with crucial effects on the determination of vertical profiles of extinction and an increase of the AOT by a factor of up to 3.5. Worldwide observations of CALIOP at other coastal regions of Mauna Loa (Pacific), Tasmania (Pacific), Ireland (Atlantic), and Cuba (Atlantic) show the same patterns in the surface-dependent aerosol subtyping of CALIOP and a probable overestimation of the AOT in coastal areas over land. In simplified radiative-transfer simulations, two scenarios of boundary aerosol conditions were considered: marine aerosol and polluted continental aerosol. At the surface, a difference of 5 to 13 W m^{-2} in the daily averaged direct solar aerosol radiative effect was found independent of the latitude and season. In ongoing investigations, global aerosol transport models might be used to estimate the global impact of a possible aerosol misidentification in coastal areas. At the same time it might be appropriate to account for the coastline effect in the CALIOP data algorithm by using the CALIPSO satellite GPS information and by introducing an additional aerosol type, e.g., mixed marine aerosol for coastal areas.

References

Althausen, D., Engelmann, R., Baars, H., Heese, B., Ansmann, A., Müller, D., and Komppula, M.: Portable Raman lidar Polly[XT] for automated profiling of aerosol backscatter, extinction, and depolarization, J. Atmos. Ocean. Technol., 26, 2366–2378, doi:10.1175/2009JTECHA1304.1, 2009.

Anderson, G. P., Clough, S. A., Kneizys, F. X., Chetwynd, J. H., and Shettle, E. P.: AFGL atmospheric constituent profiles (0.120km), 1986.

Anderson, T. L., Charlson, R. J., Winker, D. M., Ogren, J. A., and Holmén, K.: Mesoscale variations of tropospheric aerosols, J. Atmos. Sci., 60, 119–136, doi:10.1175/1520-0469(2003)060<0119:MVOTA>2.0.CO;2, 2003.

Ansmann, A. and Müller, D.: Lidar and atmospheric aerosol particles, in: Lidar: Range–resolved optical remote sensing of the atmosphere, edited by: Weitkamp, C., 105–138, Springer, 2005.

Bates, T. S., Huebert, B. J., Gras, J. L., Griffiths, F. B., and Durkee, P. A.: International Global Atmospheric Chemistry

(IGAC) Project's First Aerosol Characterization Experiment (ACE 1): Overview, J. Geophys. Res., 103, 16297–16318, doi:10.1029/97JD03741, 1998.

Blanco-Muriel, M., Alarcn-Padilla, D. C., Lopez-Moratalla, T., and Lara-Coira, M.: Computing the solar vector, Solar Energy, 70, 431–441, doi:10.1016/S0038-092X(00)00156-0, 2001.

Bridhikitti, A.: Atmospheric aerosol layers over Bangkok Metropolitan Region from CALIPSO observations, Atmos. Res., 127, 1–7, doi:10.1016/j.atmosres.2013.02.008, 2013.

Burton, S. P., Ferrare, R. A., Hostetler, C. A., Hair, J. W., Rogers, R. R., Obland, M. D., Butler, C. F., Cook, A. L., Harper, D. B., and Froyd, K. D.: Aerosol classification using airborne High Spectral Resolution Lidar measurements – methodology and examples, Atmos. Meas. Tech., 5, 73–98, doi:10.5194/amt-5-73-2012, 2012.

Burton, S. P., Ferrare, R. A., Vaughan, M. A., Omar, A. H., Rogers, R. R., Hostetler, C. A., and Hair, J. W.: Aerosol classification from airborne HSRL and comparisons with the CALIPSO vertical feature mask, Atmos. Meas. Tech., 6, 1397–1412, doi:10.5194/amt-6-1397-2013, 2013.

Draxler, R. R. and Rolph, G. D.: HYSPLIT (HYbrid Single-Particle Lagrangian Integrated Trajectory) model access via NOAA ARL READY website, http://www.arl.noaa.gov/ready/hysplit4.html (last access: 24 June 2014), NOAA Air Resources Laboratory, Silver Spring, 2003.

Dubovik, O., Holben, B., Eck, T. F., Smirnov, A., Kaufman, Y. J., King, M. D., Tanré, D., and Slutsker, I.: Variability of absorption and optical properties of key aerosol types observed in worldwide locations, J. Atmos. Sci., 59, 590–608, doi:10.1175/1520-0469(2002)059<0590:VOAAOP>2.0.CO;2, 2002.

Freudenthaler, V., Esselborn, M., Wiegner, M., Heese, B., Tesche, M., Ansmann, A., Müller, D., Althausen, D., Wirth, M., Fix, A., Ehret, G., Knippertz, P., Toledano, C., Gasteiger, J., Garhammer, M., and Seefeldner, M.: Depolarization ratio profiling at several wavelengths in pure Saharan dust during SAMUM 2006, Tellus Series B, 61, 165–179, doi:10.1111/j.1600-0889.2008.00396.x, 2009.

Groß, S., Esselborn, M., Weinzierl, B., Wirth, M., Fix, A., and Petzold, A.: Aerosol classification by airborne high spectral resolution lidar observations, Atmos. Chem. Phys., 13, 2487–2505, doi:10.5194/acp-13-2487-2013, 2013.

Holben, B. N., Eck, T. F., Slutsker, I., Tanre, D., Buis, J. P., Setzer, A., Vermote, E., Reagan, J. A., Kaufman, Y. J., Nakajima, T., Lavenu, F., Jankowiak, I., and Smirnov, A.: AERONET–A federated instrument network and data archive for aerosol characterization, Remote Sens. Environ., 66, 1–16, doi:10.1016/S0034-4257(98)00031-5, 1998.

Holben, B. N., Tanr'e, D., Smirnov, A., Eck, T. F., Slutsker, I., Abuhassan, N., Newcomb, W. W., Schafer, J. S., Chatenet, B., Lavenu, F., Kaufman, Y. J., Vande Castle, J., Setzer, A., Markham, B., Clark, D., Frouin, R., Halthore, R., Karneli, A., O'Neill, N. T., Pietras, C., Pinker, R. T., Voss, K., and Zibordi, G.: An emerging ground-based aerosol climatology: Aerosol optical depth from AERONET, J. Geophys. Res., 106, 12067–12097, doi:10.1029/2001JD900014, 2001.

Huang, J., Fu, Q., Su, J., Tang, Q., Minnis, P., Hu, Y., Yi, Y., and Zhao, Q.: Taklimakan dust aerosol radiative heating derived from CALIPSO observations using the Fu-Liou radiation model with CERES constraints, Atmos. Chem. Phys., 9, 4011–4021, doi:10.5194/acp-9-4011-2009, 2009.

IGBP: The International Geosphere-Biosphere Programme: a study of global change-the initial core project, IGBP Global Change Report no. 12, International Geosphere-Biosphere Programme, Stockholm, Sweden, available at: http://www-surf.larc.nasa.gov/surf/pages/sce_type_A.html (last access: 10 May 2014), 1990.

Kahn, R. A., Chen, Y., Nelson, D. L., Leung, F. Y., Li, Q., Diner, D. J., and Logan, J. A.: Wildfire smoke injection heights: Two perspectives from space, Geophys. Res. Lett., 35, L04809, doi:10.1029/2007GL032165, 2008.

Kanitz, T., Seifert, P., Ansmann, A., Engelmann, R., Althausen, D., Casiccia, C., and Rohwer, E. G.: Contrasting the impact of aerosols at northern and southern midlatitudes on heterogeneous ice formation, Geophys. Res. Lett., 38, L17802, doi:10.1029/2011GL048532, 2011.

Kanitz, T., Ansmann, A., Engelmann, R., and Althausen, D.: North–south cross sections of aerosol layering over the Atlantic Ocean from multiwavelength Raman/polarization lidar during Polarstern cruises., J. Geophys. Res., 118, 2643–2655, doi:10.1002/jgrd.50273, 2013.

Kato, S., Ackerman, T. P., Mather, J. H., and Clothiaux, E. E.: The k–distribution method and correlated–k approximation for a shortwave radiative transfer model, J. Quant. Spectr. Radiat. Trans., 62, 109–121, doi:10.1016/S0022-4073(98)00075-2, 1999.

Kylling, A.: Radiation transport in cloudy and aerosol loaded atmospheres, Ph.D. thesis, Alaska University, Fairbanks, 1992.

Liu, D., Wang, Z., Liu, Z., Winker, D., and Trepte, C.: A height resolved global view of dust aerosols from the first year CALIPSO lidar measurements, J. Geophys. Res., 113, D16214, doi:10.1029/2007JD009776, 2008.

Liu, Z., Vaughan, M., Winker, D., Kittaka, C., Getzewich, B., Kuehn, R., Omar, A., Powell, K., Trepte, C., and Hostetler, C.: The CALIPSO lidar cloud and aerosol discrimination: Version 2 algorithm and initial assessment of performance, J. Atmos. Ocean. Technol., 26, 1198–1213, doi:10.1175/2009JTECHA1229.1, 2009.

Lopes, F. J. S., Landulfo, E., and Vaughan, M. A.: Evaluating CALIPSO's 532 nm lidar ratio selection algorithm using AERONET sun photometers in Brazil, Atmos. Meas. Tech., 6, 3281–3299, doi:10.5194/amt-6-3281-2013, 2013.

Mamouri, R. E., Amiridis, V., Papayannis, A., Giannakaki, E., Tsaknakis, G., and Balis, D. S.: Validation of CALIPSO spaceborne-derived attenuated backscatter coefficient profiles using a ground-based lidar in Athens, Greece, Atmos. Meas. Tech., 2, 513–522, doi:10.5194/amt-2-513-2009, 2009.

Mayer, B. and Kylling, A.: Technical note: The libRadtran software package for radiative transfer calculations - description and examples of use, Atmos. Chem. Phys., 5, 1855-1877, doi:10.5194/acp-5-1855-2005, 2005.

Miller, S. T. K., Keim, B. D., Talbot, R. W., and Mao, H.: Sea breeze: Structure, forecasting, and impacts, Rev. Geophys., 41, 1011, doi:10.1029/2003RG000124, 2003.

Omar, A. H., Winker, D. M., Kittaka, C., Vaughan, M. A., Liu, Z., Hu, Y., Trepte, C. R., Rogers, R. R., Ferrare, R. A., Lee, K. P., Kuehn, R. E., and Hostetler, C. A.: The CALIPSO automated aerosol classification and lidar ratio se-

lection algorithm, J. Atmos. Ocean. Technol., 26, 1994–2014, doi:10.1175/2009JTECHA1231.1, 2009.

Omar, A. H., Winker, D. M., Tackett, J. L., Giles, D. M., Kar, J., Liu, Z., Vaughan, M. A., Powell, K. A., and Trepte, C. R.: CALIOP and AERONET aerosol optical depth comparisons: One size fits none, J. Geophys. Res., 118, 4748–4766, doi:10.1002/jgrd.50330, 2013.

Oomar, M. and Holz, R.: Improving the CALIOP aerosol optical depth using combined MODIS-CALIOP observations and CALIOP integrated attenuated total color ratio, J. Geophys. Res., 116, D14201, doi:10.1029/2010JD014894, 2011.

Rogers, R. R., Hostetler, C. A., Hair, J. W., Ferrare, R. A., Liu, Z., Obland, M. D., Harper, D. B., Cook, A. L., Powell, K. A., Vaughan, M. A., and Winker, D. M.: Assessment of the CALIPSO Lidar 532 nm attenuated backscatter calibration using the NASA LaRC airborne High Spectral Resolution Lidar, Atmos. Chem. Phys., 11, 1295–1311, doi:10.5194/acp-11-1295-2011, 2011.

Pappalardo, G., Wandinger, U., Mona, L., Hiebsch, A., Mattis, I., Amodeo, A., Ansmann, A., Seifert, P., Linné, H., Apituley, A., and other: EARLINET correlative measurements for CALIPSO: First intercomparison results, J. Geophys. Res., 115, D00H19, doi:10.1029/2009JD012147, 2010.

Schneider, C., Glaser, M., Kilian, R., Santana, A., Butorovic, N., and Casassa, G.: Weather observations across the southern Andes at 53° S, Physical Geography, 24, 97–119, 2003.

Schuster, G. L., Vaughan, M., MacDonnell, D., Su, W., Winker, D., Dubovik, O., Lapyonok, T., and Trepte, C.: Comparison of CALIPSO aerosol optical depth retrievals to AERONET measurements, and a climatology for the lidar ratio of dust, Atmos. Chem. Phys., 12, 7431–7452, doi:10.5194/acp-12-7431-2012, 2012.

Smirnov, A., Holben, B. N., Slutsker, I., Giles, D. M., McClain, C. R., Eck, T. F., Sakerin, S. M., Macke, A., Croot, P., Zibordi, G., Quinn, K., Sciare, J., Kinne, S., Harvey, M., Smyth, T. J., Piketh, S., Zielinski, T., Proshutinsky, A., Goes, J. I., Nelson, N. B., Larouche, P., Radionov, V. F., Goloub, P., Krishna Moorthy, K., Matarrese, R., Robertson, E. J., and Jourdin, F.: Maritime Aerosol Network as a component of Aerosol Robotic Network, J. Geophys. Res., 114, D06204, doi:10.1029/2008JD011257, 2009.

Stamnes, K., Tsay, S.-C., Jayaweera, K., and Wiscombe, W.: Numerically stable algorithm for discrete–ordinate–method radiative transfer in multiple scattering and emitting layered media, Atmos. Optics, 27, 2502–2509, doi:10.1364/AO.27.002502, 1988.

Tesche, M., Wandinger, U., Ansmann, A., Althausen, D., Müller, D., and Omar, A. H.: Ground–based validation of CALIPSO observations of dust and smoke in the Cape Verde region, J. Geophys. Res., 118, 2889–2902, doi:10.1002/jgrd.50248, 2013.

Várnai, T., Marshak, A., and Yang, W.: Multi-satellite aerosol observations in the vicinity of clouds, Atmos. Chem. Phys., 13, 3899–3908, doi:10.5194/acp-13-3899-2013, 2013.

Vaughan, M. A., Powell, K. A., Kuehn, R. E., Young, S. A., Winker, D. M., Hostetler, C., Hunt, W. H., Liu, Z., McGill, M. J., and Getzewich, B. J.: Fully Automated Detection of Cloud and Aerosol Layers in the CALIPSO Lidar Measurements, J. Atmos. Ocean. Technol., 26, 2034–2050, doi:10.1175/2009JTECHA1228.1, 2009.

Wandinger, U., Tesche, M., Seifert, P., Ansmann, A., Müller, D., and Althausen, D.: Size matters: Influence of multiple–scattering on CALIPSO light–extinction profiling in desert dust, Geophys. Res. Lett., 37, L10801, doi:10.1029/2010GL042815, 2010.

Wilson, S. R. and Forgan, B. W.: Aerosol optical depth at Cape Grim, Tasmania 1986–1999, J. Geophys. Res., 107, 4068, doi:10.1029/2001JD000398, 2002.

Winker, D. M., Vaughan, M. A., Omar, A., Hu, Y., Powell, K. A., Liu, Z., Hunt, W. H., and Young, S. A.: Overview of the CALIPSO mission and CALIOP data processing algorithms, J. Atmos. Ocean. Technol., 26, 2310–2323, doi:10.1175/2009JTECHA1281.1, 2009.

Winker, D. M., Tackett, J. L., Getzewich, B. J., Liu, Z., Vaughan, M. A., and Rogers, R. R.: The global 3-D distribution of tropospheric aerosols as characterized by CALIOP, Atmos. Chem. Phys., 13, 3345–3361, doi:10.5194/acp-13-3345-2013, 2013.

Young, W., Marshak, A., Varnai, T., and Liu, Z.: Effect of CALIPSO cloud aerosol discrimination (CAD) confidence levels on observations of aerosol properties near clouds, Atmos. Res., 54, 742–753, doi:10.1016/j.atmosres.2012.03.013, 2012.

Young, S. A. and Vaughan, M. A.: The retrieval of profiles of particulate extinction from Cloud–Aerosol Lidar Infrared Pathfinder Satellite Observations (CALIPSO) data: Algorithm description, J. Atmos. Ocean. Technol., 26, 1105–1119, doi:10.1175/2008JTECHA1221.1, 2009.

Young, S. A., Vaughan, M. A., Kuehn R. E., and Winker, D. M.: The Retrieval of Profiles of Particulate Extinction from Cloudâ Aerosol Lidar and Infrared Pathfinder Satellite Observations (CALIPSO) Data: Uncertainty and Error Sensitivity Analyses, J. Atmos. Ocean. Technol., 30, 395–428, doi:10.1175/JTECH-D-12-00046.1, 2013.